

SEP 20 1949

~~CONFIDENTIAL~~

UNCLASSIFIED

6

Copy  
RM L9D01

NACA RM L9D01

11955  
NACA 17  
c.2



# RESEARCH MEMORANDUM

PRELIMINARY WIND-TUNNEL INVESTIGATION AT HIGH-SUBSONIC  
SPEEDS OF PLANING-TAIL, BLENDED, AND  
AIRFOIL-FOREBODY SWEEP HULLS

By John M. Riebe and Richard G. MacLeod

Langley Aeronautical Laboratory  
Langley Air Force Base, Va.

CLASSIFICATION CANCELLED

CLASSIFIED DOCUMENT

Authority NACA R 92471 Date 8/2/54

By doty 9/2/54 See

This document contains classified information affecting the National Defense of the United States within the meaning of the Espionage Act, USC 50:31 and 32. Its transmission or the revelation of its contents in any manner to an unauthorized person is prohibited by law. Information so classified may be imparted only to persons in the military and naval service of the United States, appropriate civilian officers and employees of the Federal Government who have a legitimate interest therein, and to United States citizens of known loyalty and discretion who of necessity must be informed thereof.

## NATIONAL ADVISORY COMMITTEE FOR AERONAUTICS

WASHINGTON  
September 12, 1949

UNCLASSIFIED

~~CONFIDENTIAL~~

NACA LIBRARY  
LANGLEY AERONAUTICAL LABORATORY  
HAMPSHIRE, VA.



UNCLASSIFIED

## NATIONAL ADVISORY COMMITTEE FOR AERONAUTICS

## RESEARCH MEMORANDUM

PRELIMINARY WIND-TUNNEL INVESTIGATION AT HIGH-SUBSONIC  
SPEEDS OF PLANING-TAIL, BLENDED, AND  
AIRFOIL-FOREBODY SWEEP HULLS

By John M. Riebe and Richard G. MacLeod

## SUMMARY

A preliminary investigation was made in the Langley high-speed 7- by 10-foot tunnel to determine the high-subsonic aerodynamic characteristics of three different types of flying-boat hull: namely, a planing-tail hull, a blended hull, and an airfoil-forebody swept hull. For comparative purposes a body of revolution representative of the fuselage of a modern high-speed airplane was also included. All the hull and fuselage data presented include the forces and moments of a thin wing swept back  $51.3^\circ$  at the leading edge. The models were tested as reflection-plane half-models on the side wall of the tunnel. Mach numbers ranged from 0.48 to 0.99.

The results of the investigation, which are considered qualitative, showed agreement as to relative hull efficiency with previously reported low-speed investigations of larger-scale models. The drag-coefficient variation and pitching-moment-coefficient variation with Mach number for the hulls and wing were similar to those of the fuselage and wing; thus, the problem of designing a high-speed seaplane will probably be very little different aerodynamically from that of the landplane.

## INTRODUCTION

Because of the requirements for increased range and speed in flying boats, an investigation of the aerodynamic characteristics of flying-boat hulls as affected by hull dimensions and hull shape is being conducted at the Langley Aeronautical Laboratory. The results of several phases of this investigation at low speed are given in references 1 to 4.

The contemplated design of high-speed seaplanes has resulted in an extension of the investigation to high-subsonic Mach numbers. The high-speed aerodynamic characteristics of a high-length-beam-ratio hull derived from reference 1 have been presented in reference 5.

UNCLASSIFIED

The present investigation was made to determine the high-subsonic aerodynamic characteristics of two of the most promising of the hulls of the low-speed investigations: a planing-tail hull (reference 2), and an airfoil-forebody swept-hull (reference 4). A hull blended into the wing with generous fairing, which will be referred to as the "blended hull," similar to a hull developed by the Consolidated Vultee Aircraft Corporation was also tested in order to make a more complete coverage of possible hull types for high-speed water-based aircraft. For comparison purposes, a body of revolution representative of the fuselage of a modern high-speed airplane was included. All the hull and fuselage data presented include the forces and moments of a thin wing swept back  $51.3^\circ$  at the leading edge. The models were reflection-plane half-models tested on the side wall of the tunnel; these data are considered qualitative.

### SYMBOLS

The results of the tests are presented as standard NACA coefficients of forces and moments. Pitching-moment coefficients are given about the location (wing 25 percent M.A.C.) shown in figures 1 to 5.

The data are referred to the wind axes which are a system of axes having the origin at the center of moments shown in figures 1 to 5. The X-axis is in the plane of symmetry of the model and is parallel to the tunnel free-stream air flow. The Z-axis is in the plane of symmetry of the model and is perpendicular to the X-axis; the Y-axis is mutually perpendicular to the X-axis and Z-axis. The positive directions of the wind axes are shown in figure 6.

The coefficients and symbols are defined as follows:

$C_L$  lift coefficient  $\left( \frac{\text{Twice lift of semispan model}}{qS} \right)$

$C_D$  drag coefficient  $\left( \frac{\text{Twice drag of semispan model}}{qS} \right)$

$C_m$  pitching-moment coefficient  
 $\left( \frac{\text{Twice pitching moment of semispan model about Y-axis}}{qSc} \right)$

$q$  free-stream dynamic pressure, pounds per square foot  $(\rho V^2/2)$

$S$  twice wing area of semispan model, 0.214-square foot

$\bar{c}$	wing mean aerodynamic chord (M.A.C.), 0.279 foot $\left(\frac{2}{\pi} \int_0^{b/2} c^2 dy\right)$
V	free-stream velocity, feet per second
$\rho$	mass density of air, slugs per cubic foot
$\alpha$	angle of attack of wing chord line, degrees
i	incidence of wing chord line with respect to hull base line or fuselage center line
R	Reynolds number, based on wing mean aerodynamic chord ( $\rho V \bar{c} / \mu$ )
M	Mach number $\left(\frac{\text{Airspeed}}{\text{Speed of sound in air}}\right)$
b	twice wing span of semispan model, 0.79 foot
$\mu$	viscosity coefficient, slugs per foot-second
c	local wing chord, feet

## TESTS

## Test Conditions

The tests were made on the side-wall reflection plane of the Langley high-speed 7- by 10-foot tunnel. The reflection plane is located about 3 inches out from the tunnel wall (fig. 1) in order to place the model outside of the tunnel-wall boundary layer. The aerodynamic forces and moments on the model were measured with an electrical strain-gage balance which was sealed in a container on the tunnel side wall in order to prevent air flow around the model from the test section to the outside test chamber. Each model was fitted with a  $\frac{1}{16}$ -inch plate at the plane of symmetry (end plate, figs. 1 to 4) to minimize airfoil circulation that might develop through the small gap which separated the model from the reflection plane. Because the plane of symmetry of a midwing-fuselage combination acts as an end plate, no exposed end plate was necessary for the streamline body-wing combination (fig. 5). A small symmetrical end plate was used for the wing-alone condition and a small root fairing was used in addition to assure good flow at the wing leading edge. The root fairing consisted of a half round body faired into the wing and the end plate (fig. 1).

The aerodynamic characteristics were determined through a Mach number range from 0.48 to 0.99 and through a limited angle-of-attack

range between  $-1^{\circ}$  and  $4^{\circ}$ . The variation of test Reynolds number with Mach number for average test conditions is presented in figure 7. The Reynolds number is based on the wing mean aerodynamic chord and was computed by use of a turbulence factor of unity. The degree of turbulence of the tunnel is not known but is believed to be small because of the large contraction ratio of the tunnel.

### Corrections

No jet-boundary, blocking, or buoyancy corrections have been applied to the data because of the small size of the model as compared with the size of the tunnel test section. The data were corrected for the tare drag of the end plate when present. The corrections were determined from unpublished data that give the effect of end-plate size and shape on the end-plate drag. These data were obtained for end plates alone and do not, therefore, account for the effect of induced flow over the end plate caused by the wing or hull as the case may be.

### MODELS

The planing-tail hull (Langley tank model 221F), the streamline body, and the swept-hull (Langley tank model 237-6 SB) had the same proportions as the large low-speed test models of references 2, 3, and 4, respectively. Offsets for the reflection-plane half-models can be determined from the references by multiplying by the ratio of the lengths of the reflection-plane models to the low-speed models. Over-all dimensions for the half-hull and fuselage models incorporated on the left wing panel of a  $51.3^{\circ}$  sweptback wing are presented in figures 2 to 5. The swept hull was also tested with an extended leading edge which may be necessary on a full-scale water-based airplane in order to alleviate the structural problem of attaching the swept wing to the swept hull. Offsets for the extended leading edge of the swept hull, (fig. 4) are given in table I. The blended hull was similar to a configuration under development by the Consolidated Vultee Aircraft Corporation. Offsets for the blended hull are given in table II. This configuration will require a step (see fig. 2) for satisfactory hydrodynamic performance. For these tests the step was in the retracted position. The hull, fuselage, and wing dimensions represent scale models of 30,000-pound airplanes with wing loadings of about 34 pounds per square foot.

The volumes, surface areas, frontal areas, and side areas for the complete hulls and fuselage are presented in table III.

The hull used in determining the volume and areas of the blended model was arbitrarily considered as that portion enclosed by an extension of the dead rise to the upper wing surface as shown in station A, figure 2.

Photographs of the various hull models as tested on the reflection plane are presented in figure 8.

The  $51.3^\circ$  sweptback wing used in this investigation had an aspect ratio of 2.92, a taper ratio of about 0.5, and an NACA 65<sub>1</sub>-012 airfoil section perpendicular to the 50-percent-chord line. The wing incidence was set at  $0^\circ$  on all models except for one test at  $4^\circ$  on the swept hull to find the effect of wing incidence. The wing was constructed of beryllium copper and the half-models were mahogany.

## RESULTS AND DISCUSSION

The drag and pitching-moment coefficients of the hulls and fuselage plotted against Mach number are presented in figure 9 for angles of attack ranging from  $-1^\circ$  to  $4^\circ$ ; the drag, lift, and pitching-moment coefficients for several modifications of the swept-hull model at  $2^\circ$  angle of attack are presented in figure 10. Figure 11 gives the drag-coefficient variation and pitching-moment-coefficient variation with angle of attack at Mach numbers of 0.80 and 0.95 for the blended hull and the streamline body. Figure 12 presents the aerodynamic characteristics of the planing-tail hull in pitch at a Mach number of approximately 0.90. All the hull and fuselage data presented include the forces and moments of the  $51.3^\circ$  sweptback wing.

Although the drag coefficients do not compare directly in magnitude because of limitations of this reflection-plane setup, the values are in qualitative agreement with previously reported investigations (references 2 and 4) made at low speed of large-scale models. For example, at  $2^\circ$  angle of attack (fig. 9(c)) the drag of the streamline body was less than that of the planing-tail hull and the drag of the swept hull was less than that of the streamline body, which agrees with the relative hull efficiencies of references 2 and 4. The smaller volume (table III) of the swept hull accounted largely for its lower drag. No comparison with past work could be made for the blended hull because it was not tested in the low-speed investigation.

Very little change in drag coefficient occurred with Mach number up to 0.90 for angles of attack ranging from  $-1^\circ$  to  $2^\circ$  for most of the configurations tested (figs. 9 and 10); however, a rapid increase in drag coefficient began for the hulls above 0.90 Mach number. The start of the drag rise for the streamline body was delayed to a slightly

higher Mach number, about 0.93, and the rate of increase was less than that of the hulls.

A drag rise similar to that of the wing alone was indicated for the swept hull (figs. 9(c) and 10) with the wing-root fairing. The wing-root fairing was also used for the wing-alone condition (fig. 9(c)) because the wing-alone drag rise without the root fairing occurred sooner and was greater than expected according to previous tests of similar wings. It was felt that the adverse effects on drag were probably caused as a result of end-plate misalignment. Since this end-plate condition would not be present on a complete wing, it might, therefore, be expected that the swept-hull configuration incorporating the wing-root fairing more nearly represents the swept hull than the configuration without the fairing.

Increasing the wing incidence to  $4^\circ$  on the swept hull increased the drag coefficient over that of the  $0^\circ$  incidence configuration throughout the Mach number range tested and resulted in a drag rise at a lower Mach number, 0.83 (fig. 10). However, on a complete model the drag rise may occur later because of the probable limitation of the setup for the swept hull without the wing-root fairing, as mentioned earlier. Extending the hull leading edge (fig. 4) resulted in an increase in drag coefficient throughout the Mach number range but affected the drag rise only slightly.

Very little variation in pitching-moment coefficient occurred with Mach number for the hulls or fuselage at the angles of attack tested. The lift strain gage was not operating throughout most of the present investigation; however, it is believed that the variation of lift coefficient with Mach number for all the hulls and fuselage would be similar to the small change shown in figure 10.

The minimum drag coefficient at high Mach numbers for the streamline-body and blended-hull configurations occurred near  $0^\circ$  angle of attack (fig. 11). The drag coefficient for the planing-tail hull (fig. 12) was also minimum near  $0^\circ$  angle of attack and was less steep in variation with angle of attack than either the streamline body or blended hull, probably resulting from the smaller beam of the planing-tail hull. Longitudinal stability as shown by the pitching-moment curves of figure 11 was inherent in the wing-fuselage combination. The blended hull was neutrally stable in the positive angle-of-attack range at 25 percent mean aerodynamic chord, the center of moments for the present tests. Only small changes in longitudinal stability with Mach number were noted for the fuselage and blended-hull configurations. The longitudinal stability at a Mach number of 0.90 of the planing-tail hull (fig. 12) is about the same as that of the blended hull at Mach numbers of 0.8 and 0.95 (fig. 11).

## CONCLUDING REMARKS

The results of the present hull investigation, using reflection-plane half-models, show qualitative agreement as to relative hull efficiency with previously reported low-speed investigations of large-scale models. The drag-coefficient variation and pitching-moment-coefficient variation with Mach number for the hulls and wing were satisfactory in that drag rise was delayed to high-subsonic Mach numbers and there was very little change in pitching moment with Mach number. These coefficient variations for the hulls and wing were similar to the coefficient variations of the fuselage and wing; thus, the problem of designing a high-speed seaplane will probably be very little different aerodynamically from that of the landplane.

Langley Aeronautical Laboratory  
National Advisory Committee for Aeronautics  
Langley Air Force Base, Va.

## REFERENCES

1. Yates, Campbell C., and Riebe, John M.: Effect of Length-Beam Ratio on the Aerodynamic Characteristics of Flying-Boat Hulls. NACA TN 1305, 1947.
2. Riebe, John M., and Naeseth, Rodger L.: Aerodynamic Characteristics of Three Deep-Step Planing-Tail Flying-Boat Hulls. NACA RM L8I27, 1948.
3. Riebe, John M., and Naeseth, Rodger L.: Aerodynamic Characteristics of a Refined Deep-Step Planing-Tail Flying-Boat Hull with Various Forebody and Afterbody Shapes. NACA RM L8F01, 1948.
4. Naeseth, Rodger L., and MacLeod, Richard G.: Aerodynamic Characteristics of an Airfoil-Forebody Swept Flying-Boat Hull with a Wing and Tail Swept Back  $51.3^\circ$  at the Leading Edge. NACA RM L9F08, 1949.
5. Riebe, John M., and Naeseth, Rodger L.: High-Speed Wind-Tunnel Investigation of a Flying-Boat Hull with High Length-Beam Ratio. NACA RM L7K28, 1948.



TABLE II

OFFSETS FOR BLENDED HULL

[All dimensions are given in inches]

Station	Distance to F.P.	Keel above base line	Height of hull at center line	Distance from plane of symmetry														
				Water line, 0.10	Water line, 0.20	Water line, 0.30	Water line, 0.40	Water line, 0.50	Water line, 0.60	Water line, 0.70	Water line, 0.80	Water line, 0.90	Water line, 1.00	Water line, 1.10	Water line, 1.20	Water line, 1.30	Water line, 1.40	Water line, 1.50
F.P.	0	0.69	0.69															
1	.13	.77	.82						0.08	0.11	0.05							
2	.25	.48	.86						.16	.18	.15							
3	.5	.42	.93					.19	.25	.27	.25	0.16						
4	1.0	.25	1.05			0.07	0.21	.31	.35	.37	.37	.34	0.23					
5	1.5	.08	1.14	0.03	0.11	.20	.31	.39	.44	.46	.47	.45	.39	0.25				
6	2.0	.04	1.33	.07	.17	.29	.39	.47	.52	.55	.59	.58	.51	.43	0.21	0.13		
7	2.5	.03	1.45	.09	.21	.34	.46	.53	.61	.65	.67	.68	.66	.59	.42	.22	0.17	
8	3.0	.02	1.44	.11	.23	.38	.52	.62	.70	.77	.81	.83	.83	.77	.57	.22	.14	
9	3.5	.01	1.35	.12	.26	.40	.55	.68	.79	.88	.95	1.00	1.02	.99	.76	.19		
10	4.0	.00	1.31	.12	.27	.42	.56	.71	.84	.97	1.07	1.16	1.23	1.26	1.04	.41		
11	5.0	.00	1.34	.14	.29	.45	.60	.75	.90	1.06	1.20	1.37				.92		
12	6.0	.09	1.38	.03	.21	.39	.57	.74	.92	1.07	1.25	1.48				.97		
13	7.0	.18	1.41		.05	.23	.40	.58	.75	.92	1.09	1.30	1.60			.31	.14	
14	8.0	.27	1.45			.06	.25	.41	.59	.77	.94	1.12	1.33	1.53	.31	.24	.17	
15	8.5	.32	1.47				.16	.34	.51	.68	.89	.47	1.06	.41	.27	.22	.17	
16	9.0	.36	1.48				.08	.26	.42	.44	.39	.33	.30	.27	.24	.21	.17	0.09
17	10.0	.45	1.51					.10	.24	.23	.22	.21	.20	.18	.17	.17	.15	
18	11.0	.54	1.55						.12	.14	.13	.13	.13	.13	.13	.13	.13	.12
19	12.0	.79	1.60								.06	.08	.08	.09	.09	.09	.09	.09
20	12.79	1.63	1.63															

TABLE III  
 VOLUMES, SURFACE AREAS, MAXIMUM FRONTAL AREAS,  
 AND SIDE AREAS FOR HULL TYPES TESTED  
 [values given are for complete hull or fuselage]

Model	Volume (cu in.)	Surface area (sq in.)	Maximum frontal area (sq in.)	Side area (sq in.)
Planing-tail hull	21.49	65.50	2.75	29.82
Swept hull	10.55	41.40	2.14	15.75
Swept hull with extended leading edge	10.73	43.00	2.14	16.27
Blended hull	<sup>a</sup> 14.82	<sup>a</sup> 59.32	<sup>a</sup> 2.73	14.08
Streamline body	21.60	59.60	2.17	19.07

<sup>a</sup>Determined with dead rise extended to upper wing surface (see fig. 2).


 NACA

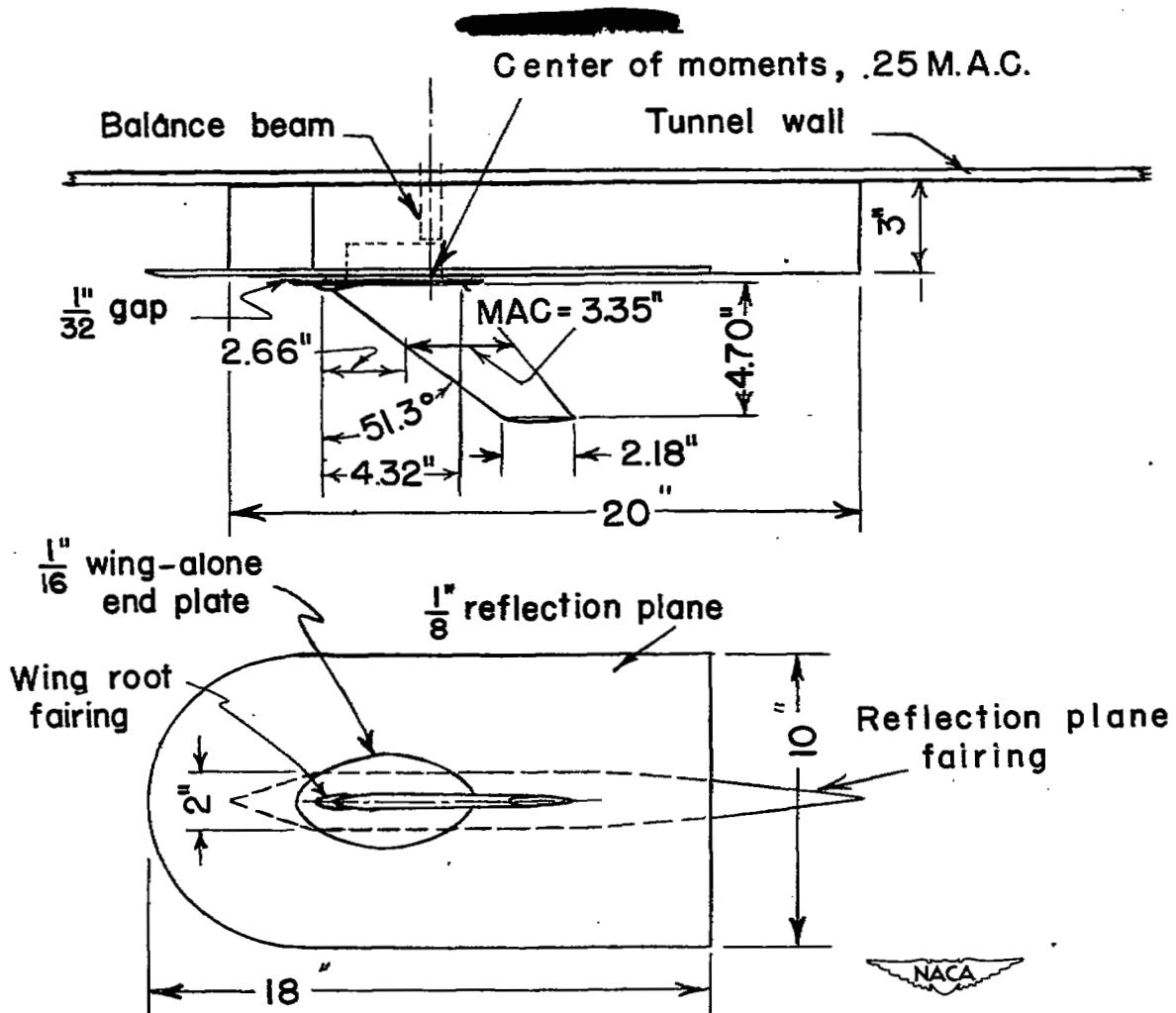


Figure 1.- Arrangement of the wall reflection plane in the Langley high-speed 7- by 10-foot tunnel; wing alone.

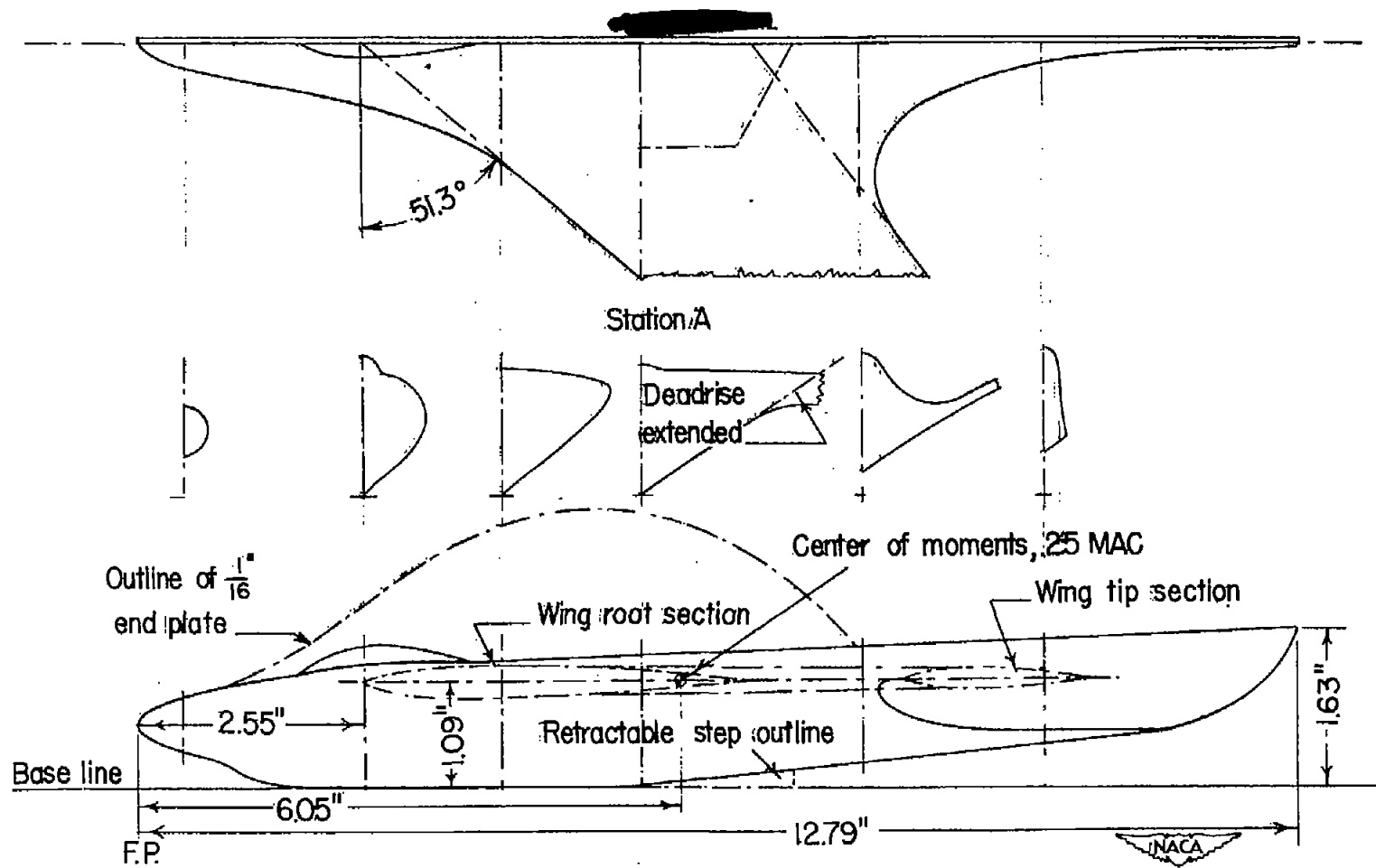


Figure 2.- Lines of reflection-plane model of blended hull.

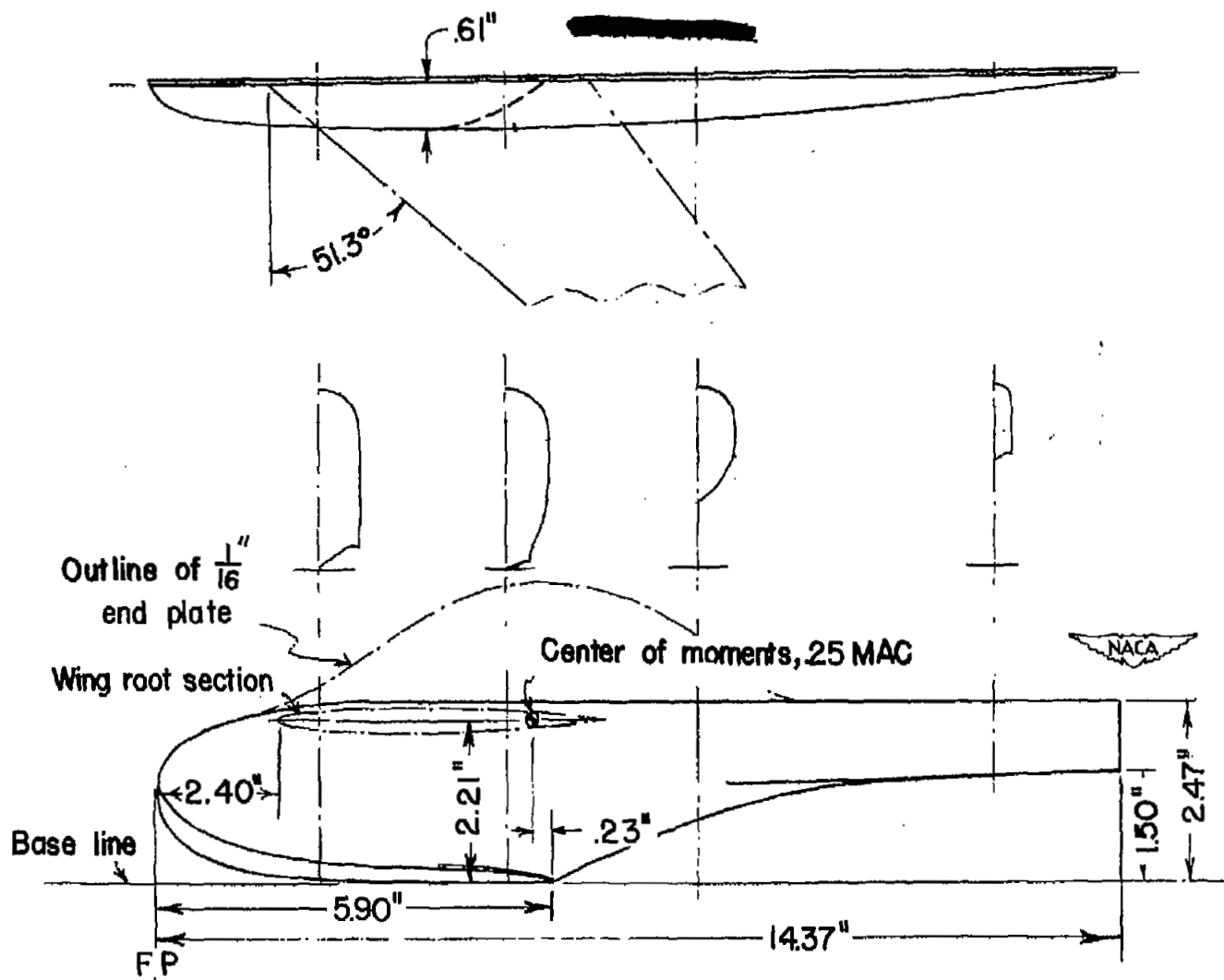


Figure 3.- Lines of reflection-plane model of planing-tail hull.

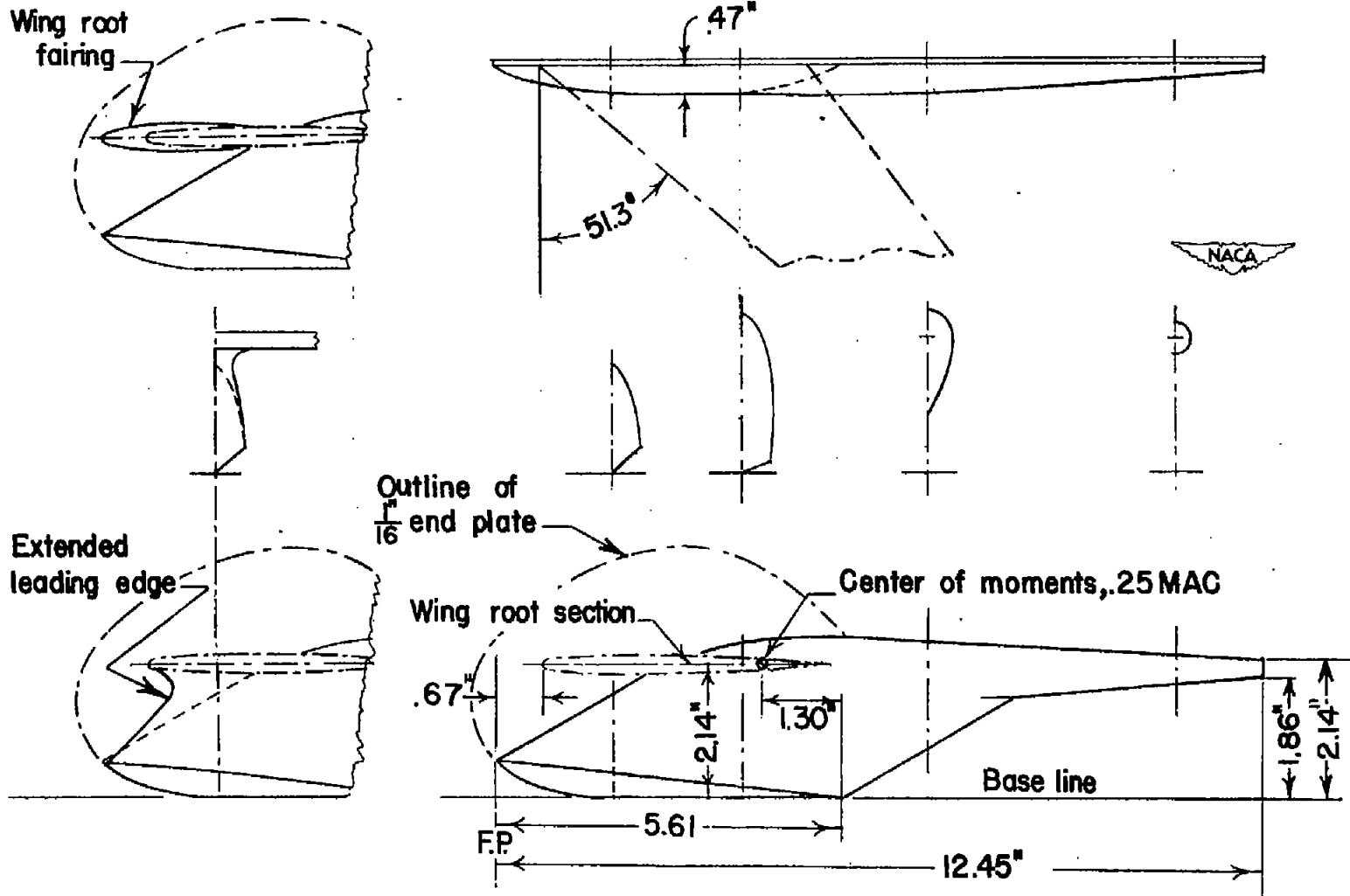


Figure 4.- Lines of reflection-plane model of sweptback hull.

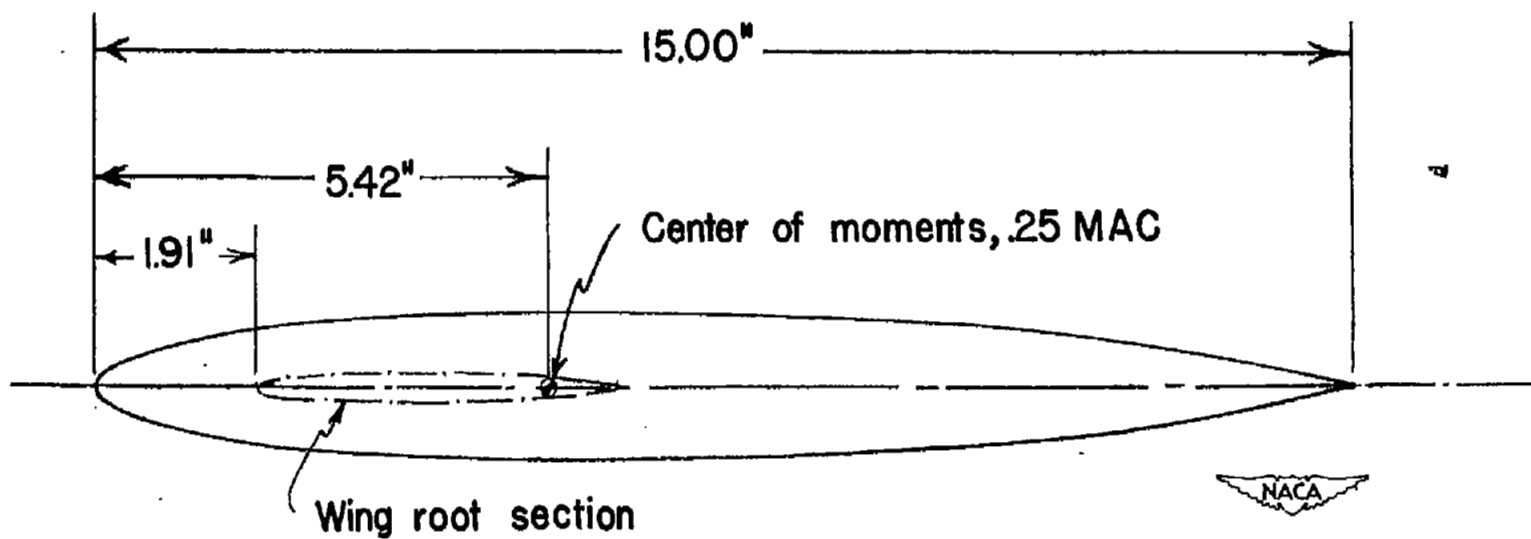
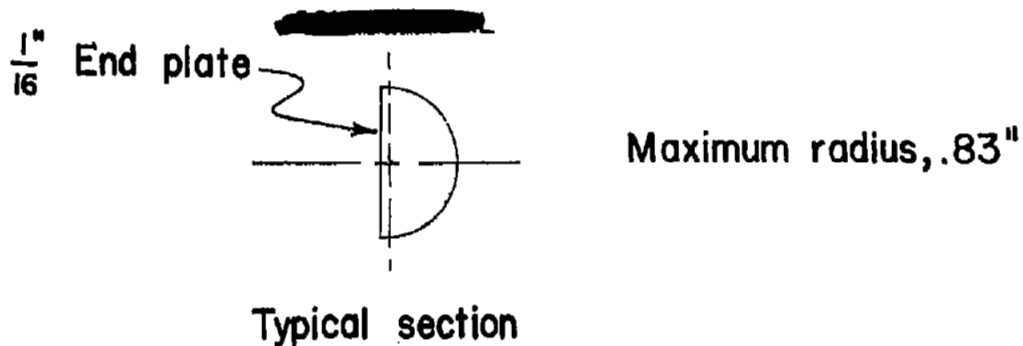


Figure 5.- Lines of streamline-body reflection-plane model.

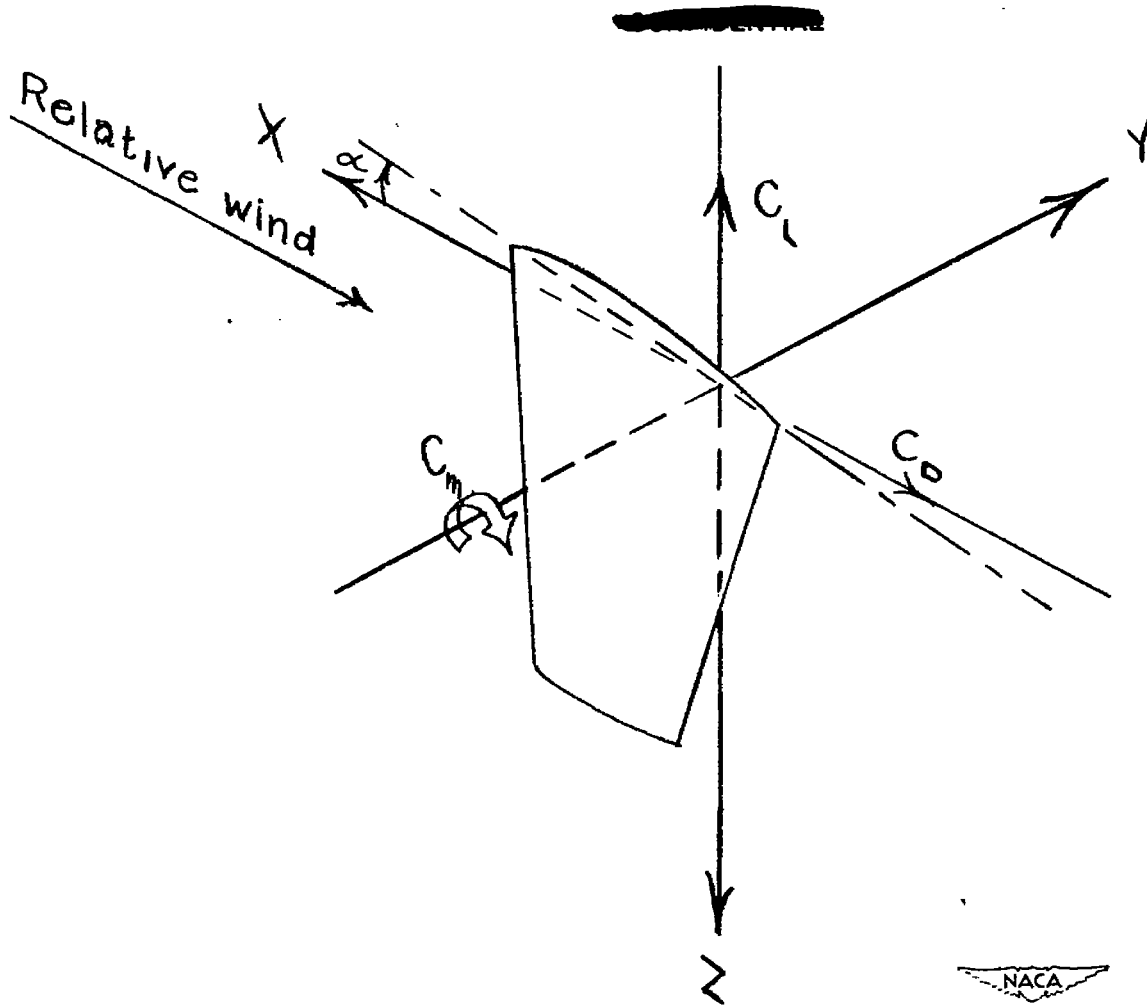


Figure 6.— Wind axes. Positive directions of forces, moments, and angles are indicated by arrows.

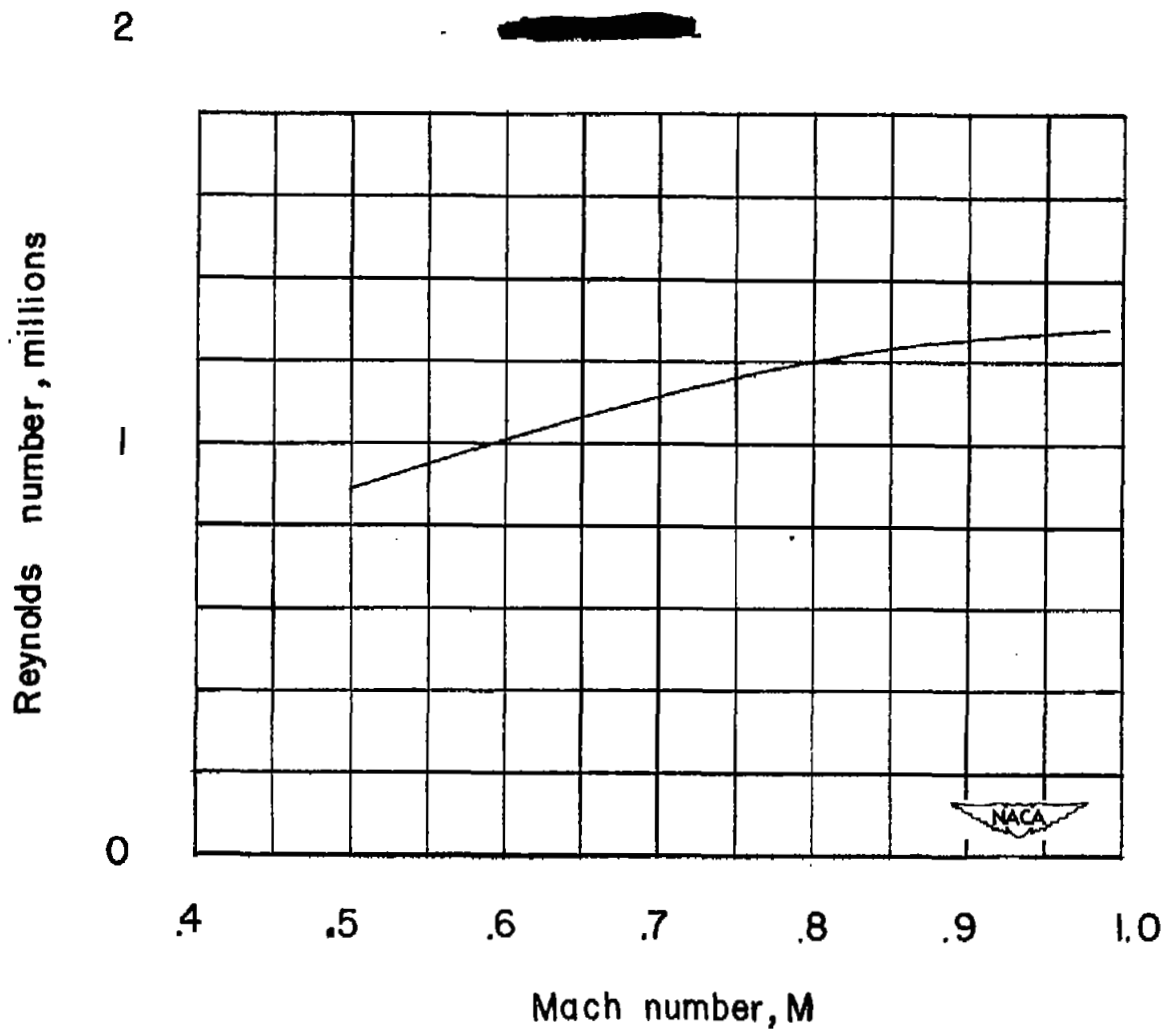
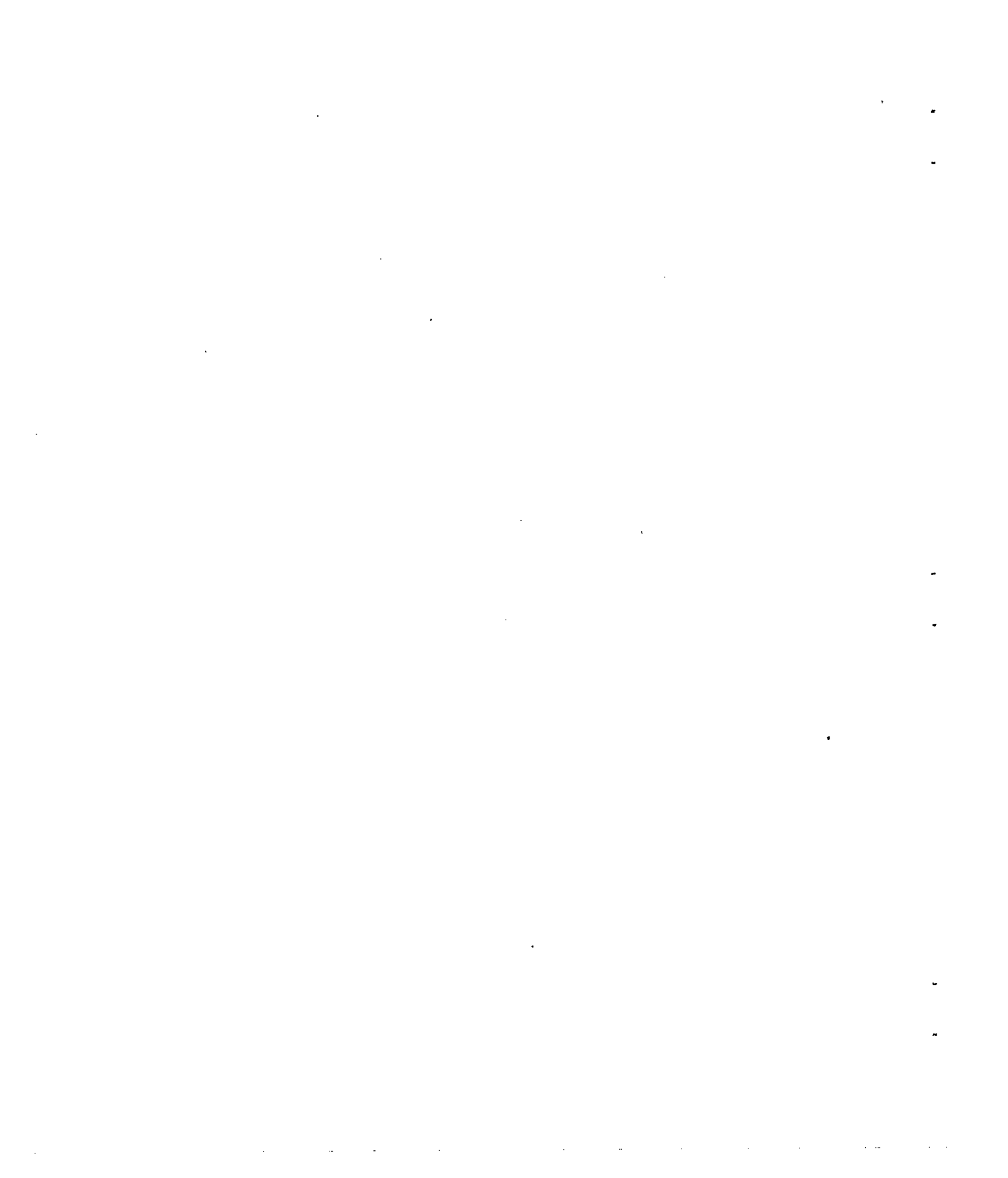
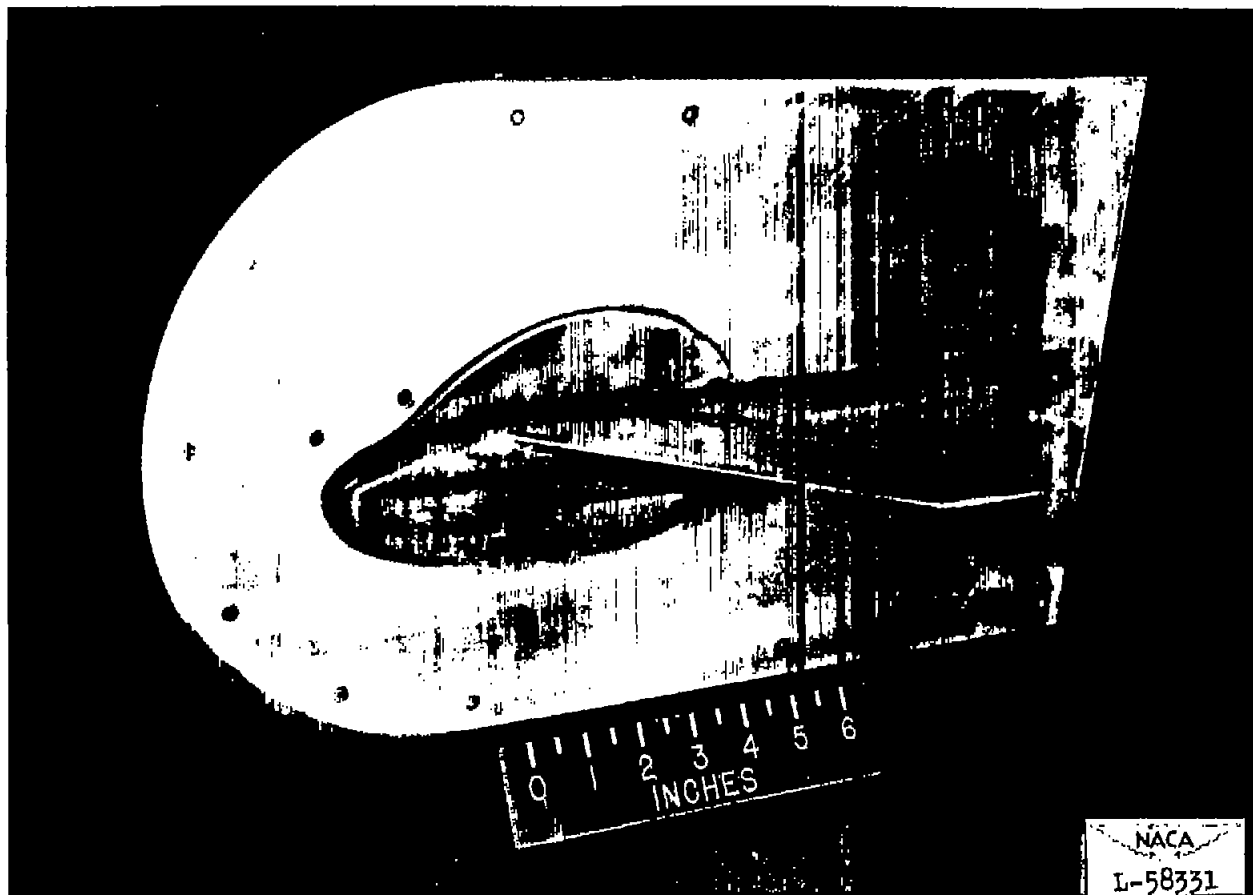


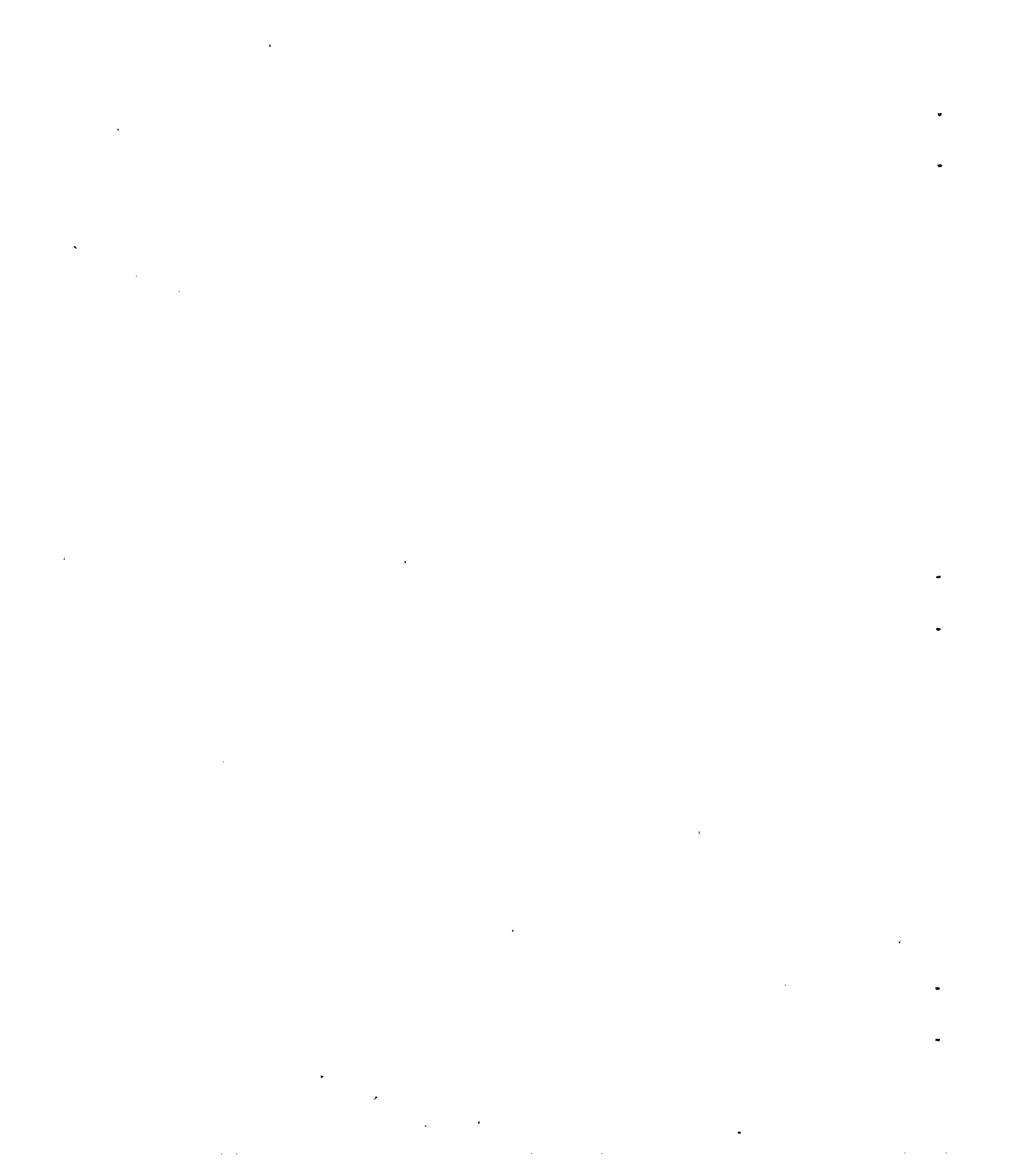
Figure 7.- Variation of test Reynolds number with Mach number for the flying-boat hulls and streamline body with a  $51.3^\circ$  sweptback wing.

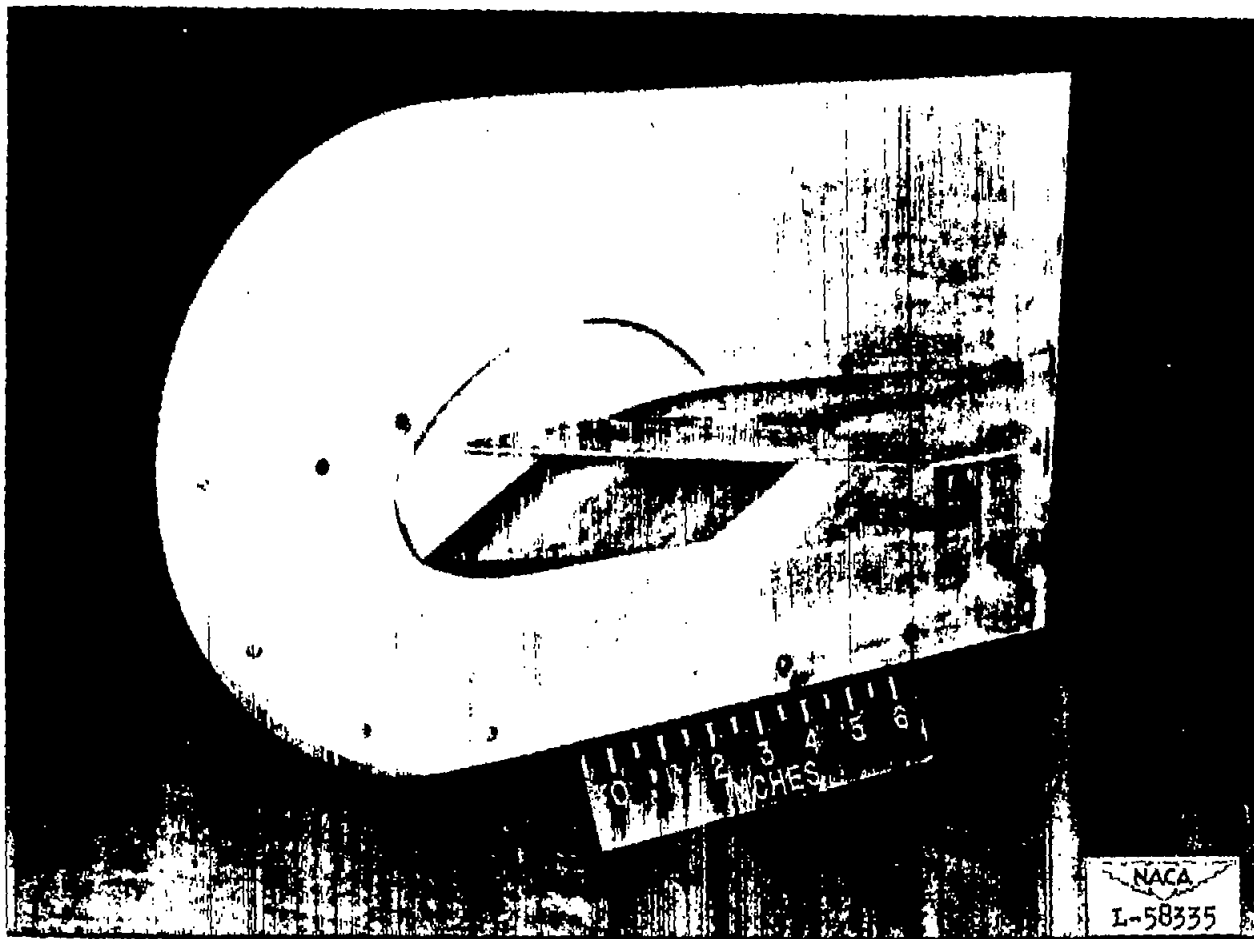




(a) Planing-tail hull.

Figure 8.- Reflection-plane hull models tested in the Langley high-speed 7- by 10-foot tunnel.

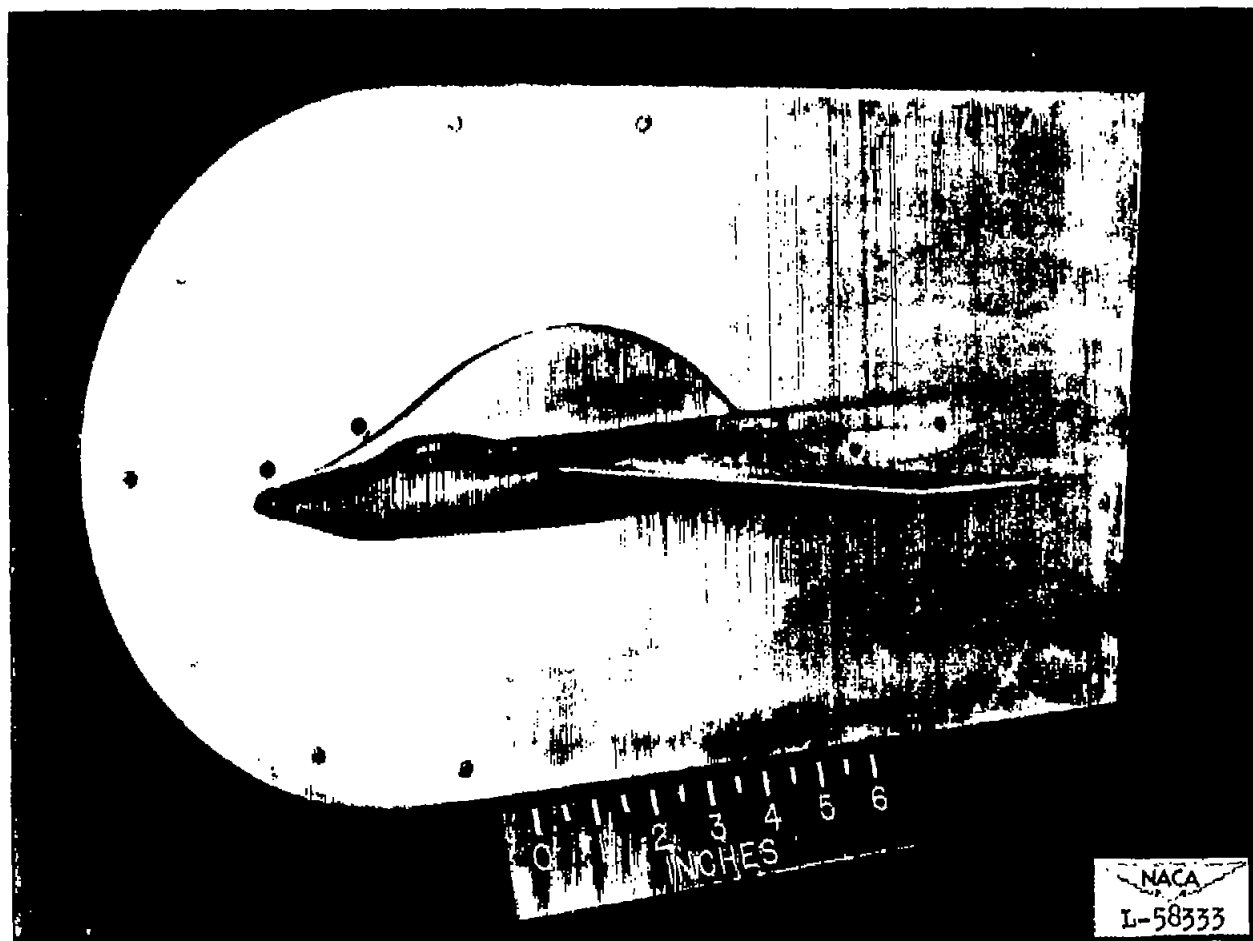




(b) Swept hull.

Figure 8.- Continued.

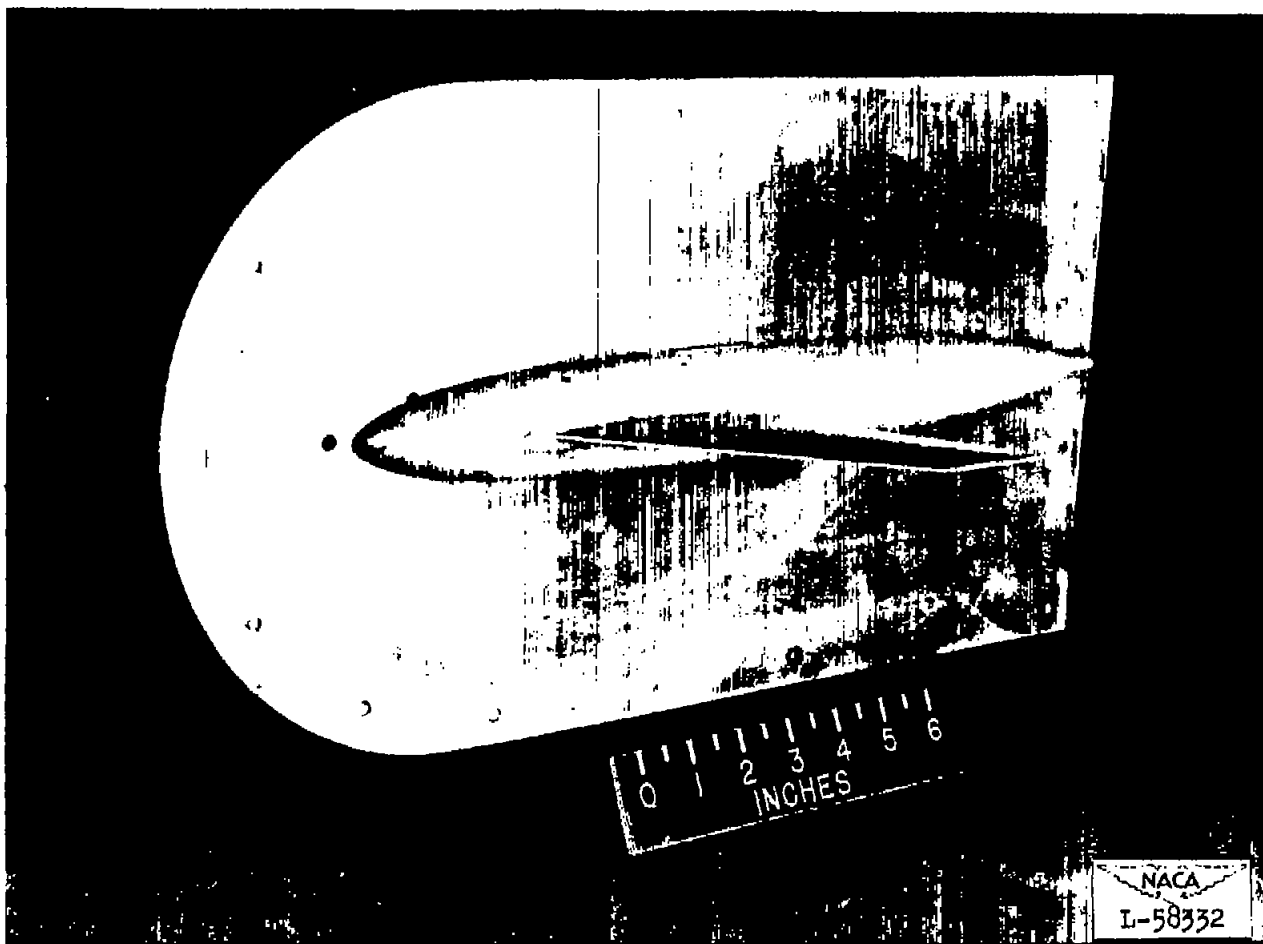




(c) Blended hull.

Figure 8.- Continued.

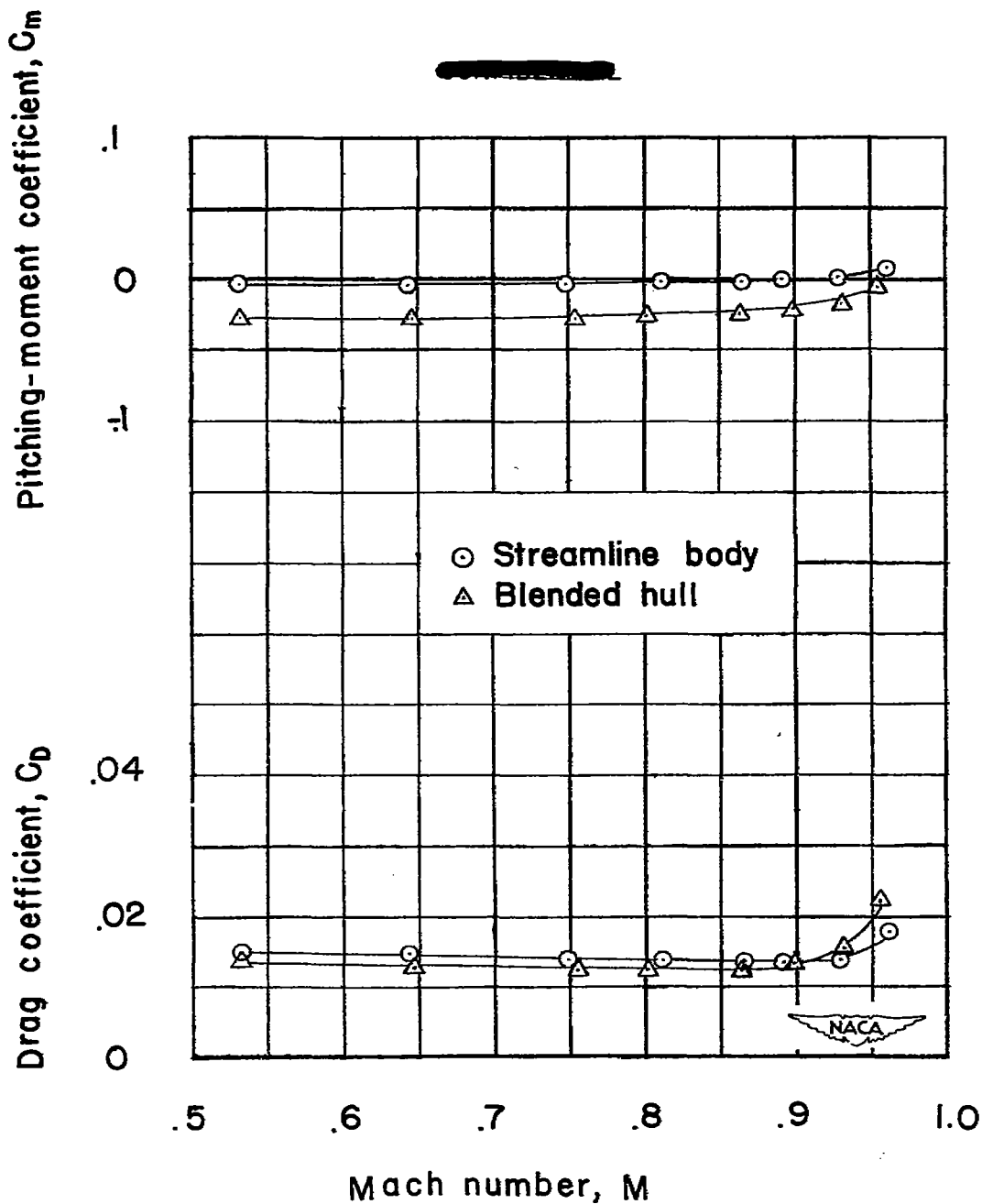




(d) Streamline body.

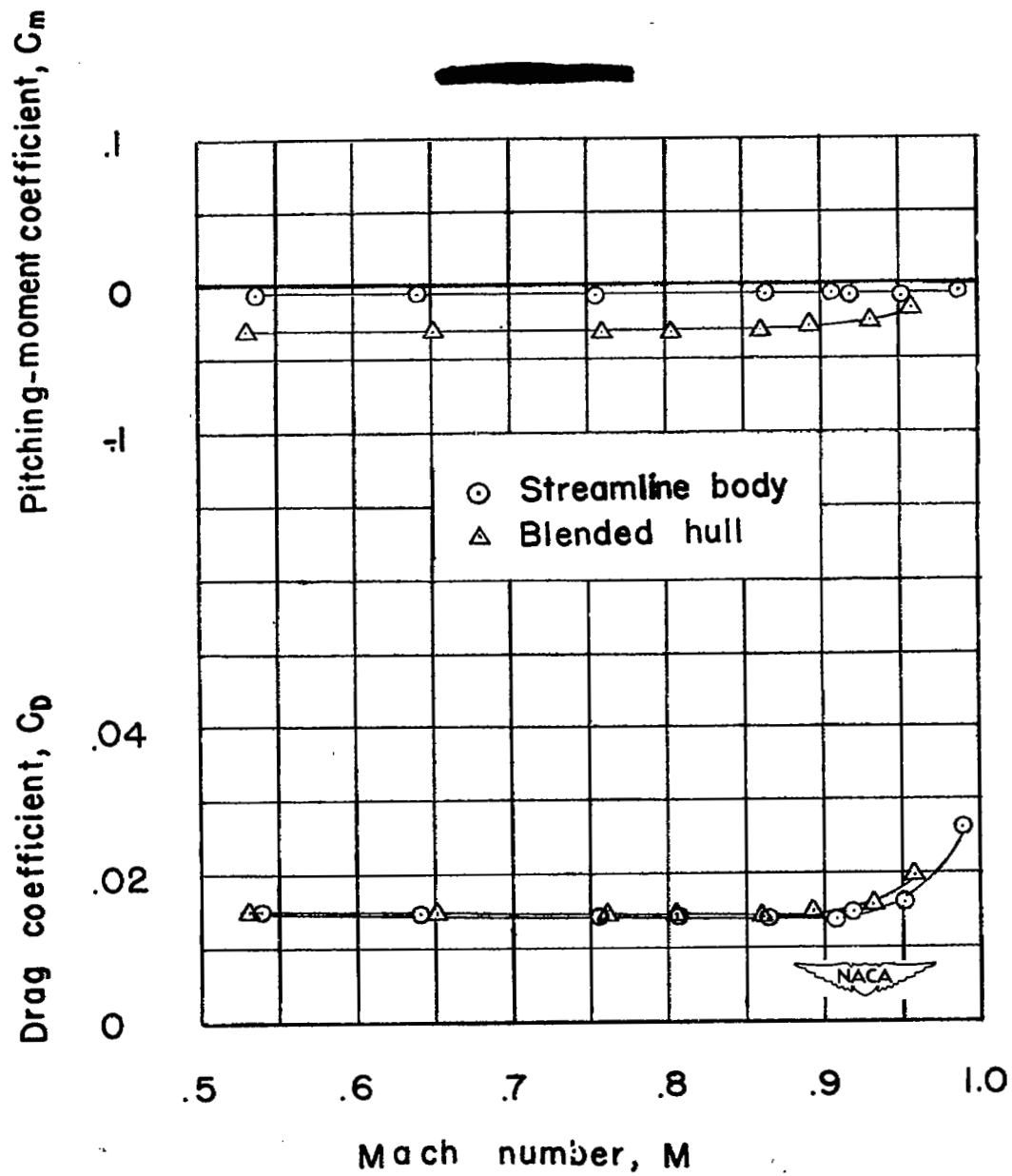
Figure 8.- Concluded.





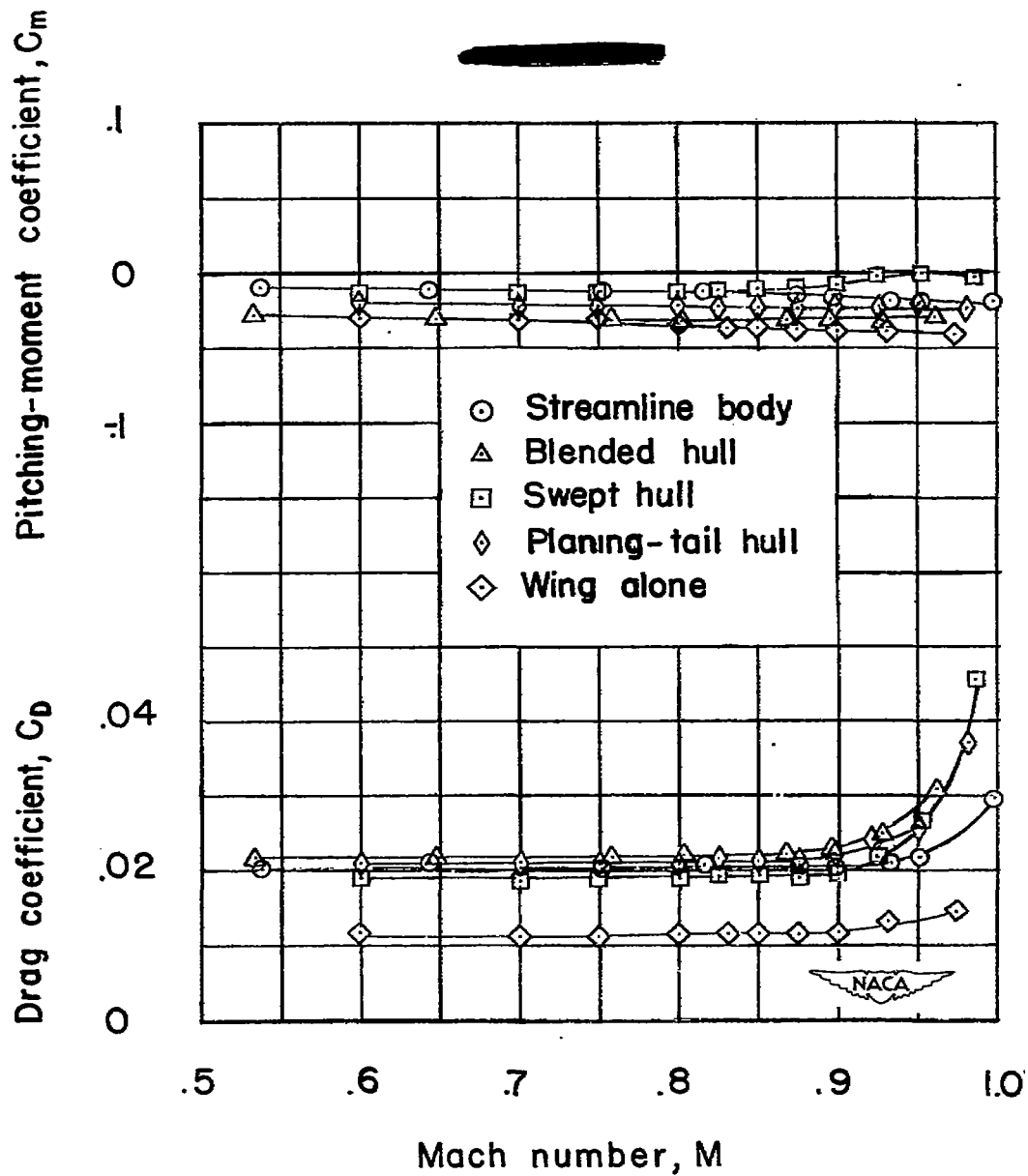
(a)  $\alpha = -1^\circ$ .

Figure 9.- Variation with Mach number of the drag coefficient and pitching-moment coefficient for several hull types and a streamline body with a  $51.3^\circ$  sweptback wing.



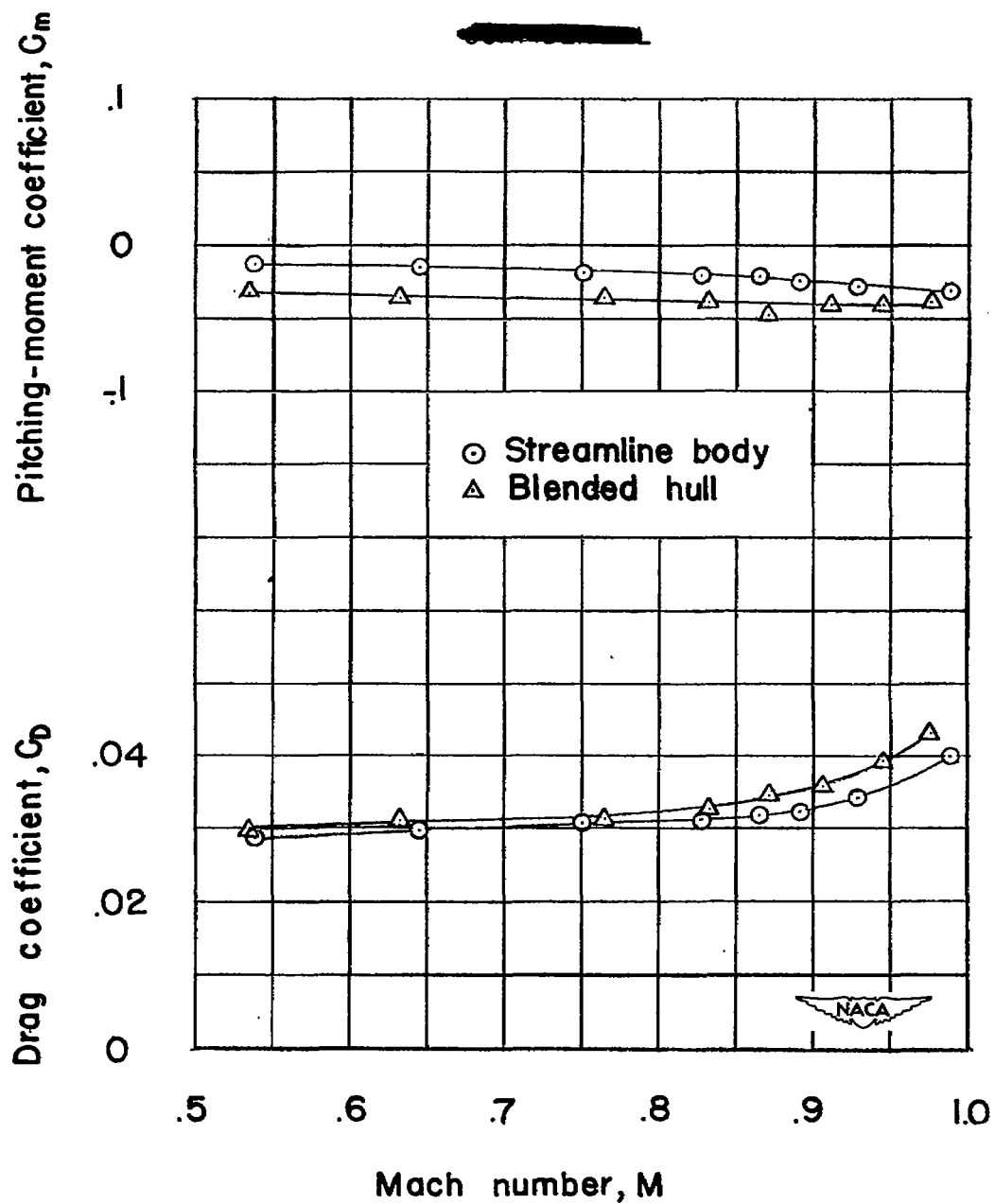
(b)  $\alpha = 0^\circ$ .

Figure 9.- Continued.



(c)  $\alpha = 2^\circ$ .

Figure 9.- Continued.



(d)  $\alpha = 4^\circ$ .

Figure 9.- Concluded.

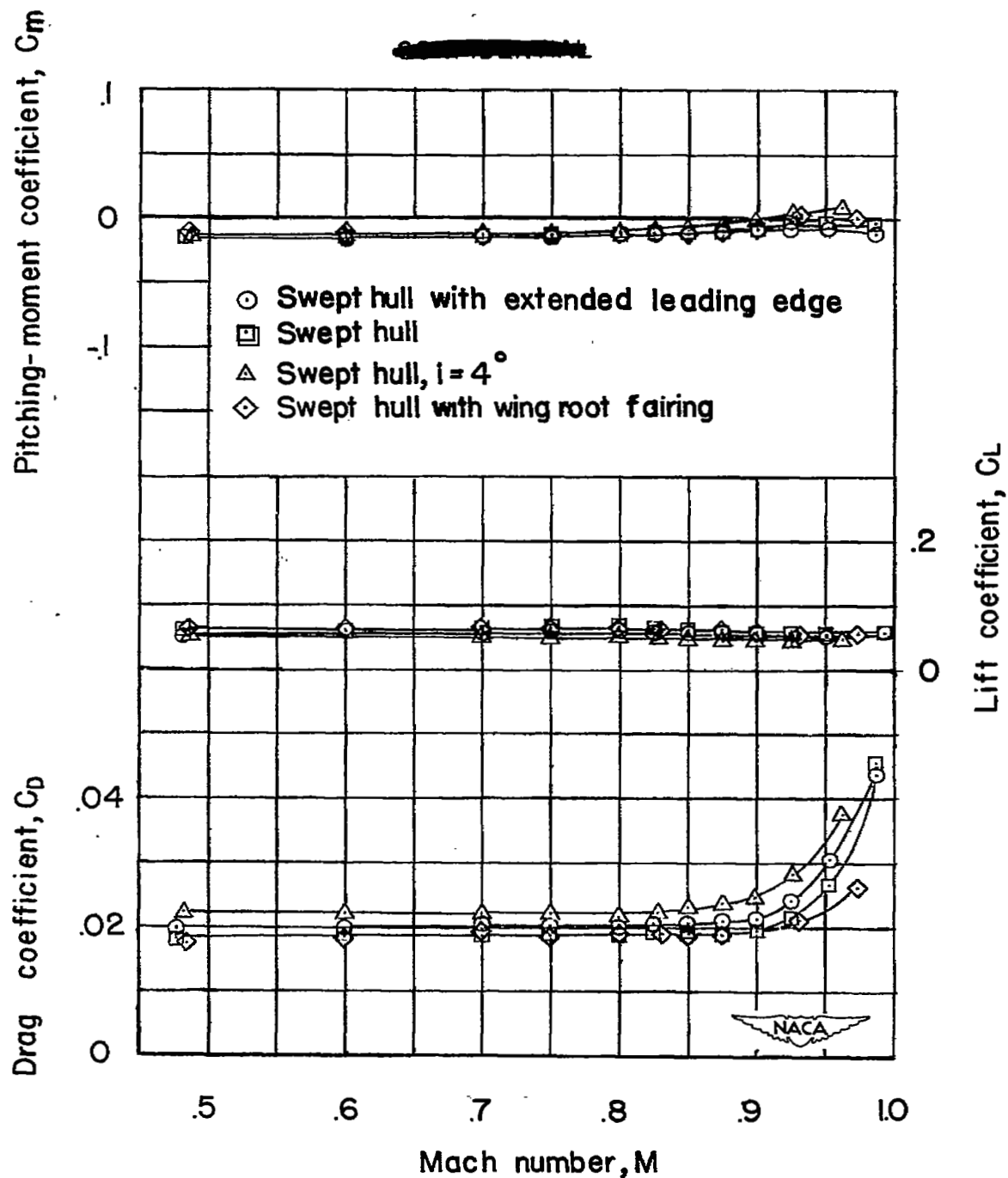


Figure 10.— Variation with Mach number of the longitudinal aerodynamic characteristics of several swept-hull configurations with a  $51.3^\circ$  sweptback wing;  $\alpha = 2^\circ$ .

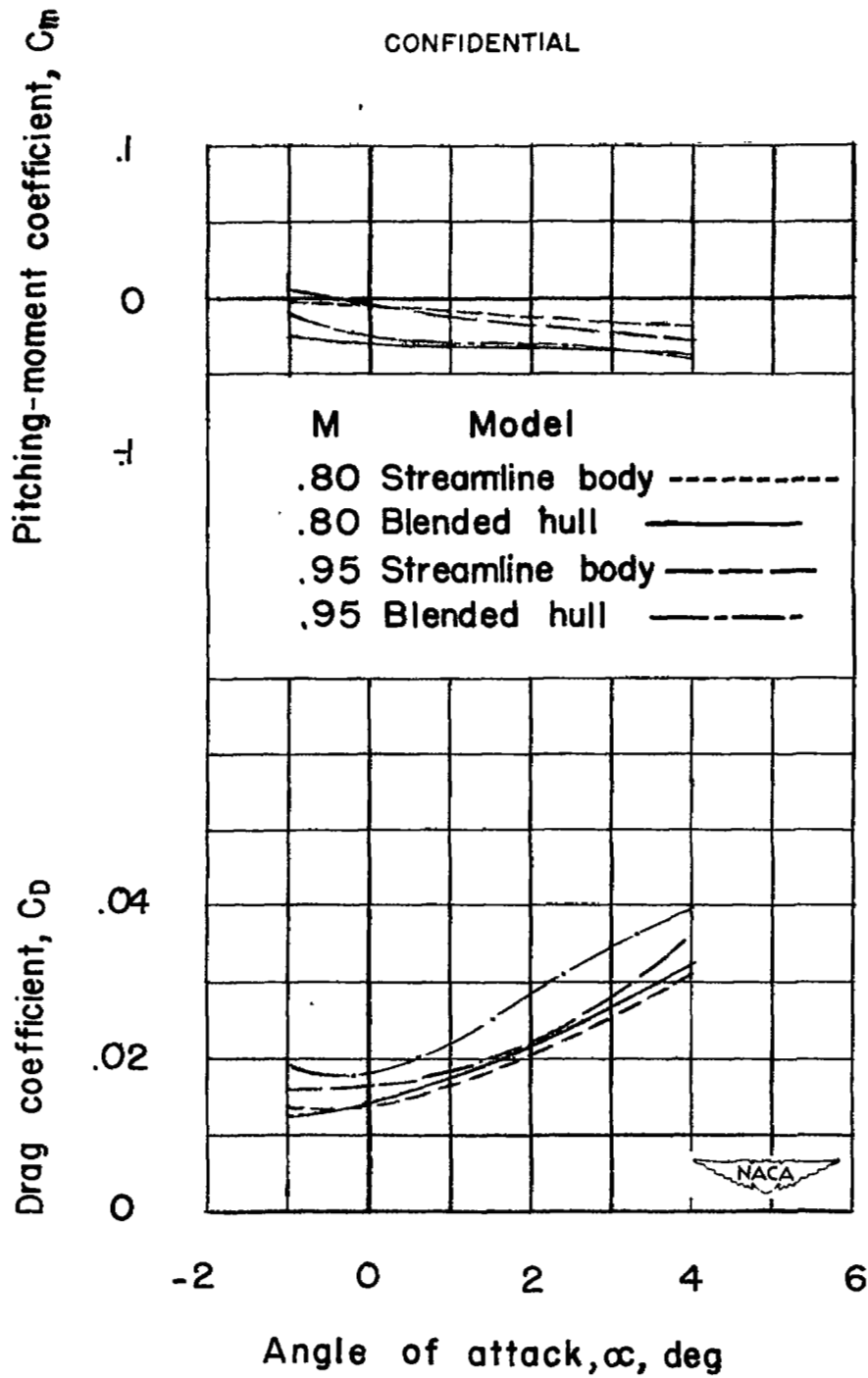


Figure 11.— Aerodynamic characteristics in pitch of a blended hull model and a streamline body with a  $51.3^\circ$  sweptback wing at Mach numbers 0.80 and 0.95.

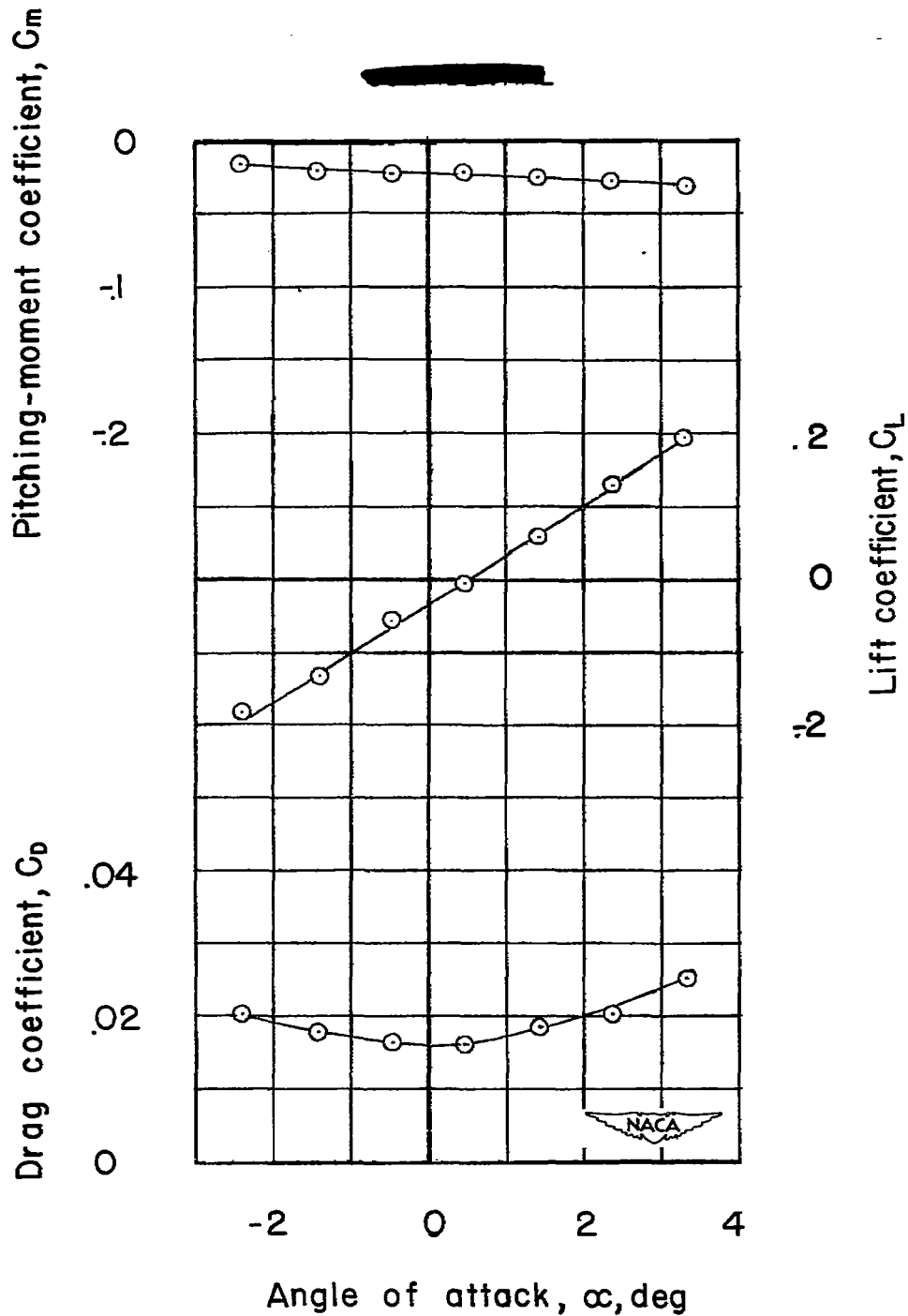


Figure 12.- Aerodynamic characteristics of planing-tail hull with a  $51.3^\circ$  sweptback wing in pitch;  $M \approx 0.90$ .

NASA Technical Library



3 1176 01436 7297

